Journal of Saudi Chemical Society (2016) **20**, 245–252

King Saud University

Journal of Saudi Chemical Society

www.ksu.edu.sa
www.sciencedirect.com

ORIGINAL ARTICLE

Offer a novel method for size appraise of NiO nanoparticles by PL analysis: Synthesis by sonochemical method

Seyid Javad Musevi [a], **Alireza Aslani** [b,c,*], **Hamid Motahari** [c], **Hassan Salimi** [d]

[a] *Department of Chemistry, Shahid Beheshti Technical Faculty, Technical and Vocational University, Urmia, Iran*
[b] *Department of Nanobiotechnology Research Center, Baqiyatallah University Medical of Science, P.O. Box 19945-546, Tehran, Iran*
[c] *Department of Basic Science, Jundi-Shapur University of Technology, P.O. Box 64615-334, Dezful, Iran*
[d] *Textile Engineering Department, Amir-Kabir University of Technology, Tehran, Iran*

Received 9 October 2011; accepted 11 June 2012
Available online 25 July 2012

KEYWORDS

Size effect;
Photoluminescence;
NiO nanoparticles

Abstract In this work, we will discuss the optical properties of NiO nanoparticles that we have investigated recently by photoluminescence (PL) spectroscopy. In particular, we will show the blue-shifts of PL, originating from the electron–hole recombination of the self-trapped exciton (STE), observed in smaller-sized NiO nanoparticles. To explain the size effect in relating to the STE PL shift, a question has been raised on whether it is appropriate to apply him quantum confinement (QC) theory usually used for the Mott-Winner type excitons in semiconductors to wide band-gap material, such as silica. Variations in several parameters and their effects on the structural (crystal size and morphology) properties of nanoparticles were investigated. Characterizations were carried out by X-ray diffraction (XRD), scanning electron microscopy (SEM), thermal stability (TGA and DTA), solid state UV and solid state florescent (PL).

1. Introduction

Tremendous amount of research effort has been made recently for the studies of nanometer-sized materials. From industrial point of view, it has always been a dream to reduce the size of electronic devices. Aiming at this goal, a great deal of interest in the research of nanoscale materials has been aroused. The successful development of this nano-research will have dramatic impact on people's daily life. Looking at this nano-study from an academic angle, understanding the chemical, physical, mechanical and optical properties of nanoscale materials is bridging a gap of knowledge between free molecules and bulk materials. In addition, important applications of NiO include preparation of cathode materials of alkaline bat-

* Corresponding author at: Department of Nanobiotechnology Research Center, Baqiyatallah University Medical of Science, P.O. Box 19945-546, Tehran, Iran. Tel.: +98 9161161165/641 6268000; fax: +98 641 6260993.
E-mail addresses: Erkin_Musevi@hotmail.com (S.J. Musevi), a.aslani110@yahoo.com, nanochemistry@yahoo.com, aslani@jsu.ac.ir (A. Aslani).
Peer review under responsibility of King Saud University.

ELSEVIER Production and hosting by Elsevier

http://dx.doi.org/10.1016/j.jscs.2012.06.009
1319-6103

teries, anti-ferromagnetic layers, and p-type transparent conducting films (Pejova et al., 2000). Nano-structured nickel(II) oxide is a p-type semiconductor metal oxide having a stable wide band gap. Also it can be used as a transparent p-type semiconductor layer (Sato et al., 1993). Furthermore, it exhibits anodic electrochromism and is utilized for applications in smart windows, electrochemical super-capacitors (Bandara and Yasomanee, 2007; Liao et al., 2006), and dye-sensitized photo cathodes (Liu and Anderson, 1996). However, the functional properties of NiO vis-a-vis its applicability significantly depend on pore morphology, pore matrix-interface, and also porosity. For example, in catalytic applications the available specific surface area should be as high as possible while for the application as a cathode material, a dense material is desirable. Initial virgin powder possesses a large surface area relative to its volume. This surface area/surface energy provides the driving force for sintering, i.e., reduction of free surface energy resulting from the high surface area of particles (Srinivasan and Weidner, 1997). NiO is a typical wide band-gap insulator (the band-gap of bulk size $E_g \cong 3.62$ eV). Therefore, the bulk NiO-based material is characterized by high transparency in ultraviolet spectral range resulting in many important technological applications. The properties of this bulky material have been extensively studied for an appreciable length of time and also been quite well established. On the other hand, modern nanoscale technology requires the production of nanometer-sized NiO films and layers, which are of frequent use in electronic devices for passivation and electrical insulation. A typical example is the design of combined NiO systems, such as metal–oxide-semiconductor (MOS). The thickness of NiO layers existing in these combined systems usually ranges several nanometers. Since the properties of NiO-based nanoscale materials are somewhat different from those of the bulk, a great body of investigations has recently been devoted to the study of nanoscaled NiO-objects. Recently, the sonochemical methods have been shown to be very promising in the preparation of a variety of materials with nanometer dimensions, including nanochalcogenides (Wang and Gu, 2006; Xu et al., 2006), metallic nanoparticles (Zhang et al., 2006; Lei et al., 2007) and nano-sized metal oxides (Kumar and Kim, 2006; Suslick et al., 1996). These materials possess improved magnetic properties (Zhou and Zhou, 2005), energy storage capacities (Song et al., 2005; Zhu et al., 2000; Yu et al., 2002), photocatalytic and catalytic properties (Suslick, 1998). The ultrasonic irradiation of liquids results in acoustic cavitation. Which, in turn, causes the formation, growth and implosive collapse of bubbles? The implosive collapse of bubbles generates localized hot spots through adiabatic compression or shock wave formation within the bubble gas phase. The conditions formed in these hot spots include transient temperatures of approximately 5000 K, transient pressures of about 1800 atm and cooling rates of 10^{10} K s^{-1} (He, 1999). These extreme conditions attained during the bubble collapse promote the formation of nano-phase materials with interesting properties. On the other hand ultrasonic irradiation has proven to be a versatile and promising tool for the development of new processes in the chemical industry (Kingery et al., 1976; Curri et al., 2002). Its unique character predominantly arises from acoustic cavitation, i.e. the growth and subsequent adiabatic collapse of a microscopic cavity in a liquid, leading to a momentary increase of temperature and pressure. These extreme local conditions can cause bond breakage and free radical formation, thereby providing an alternative route for inducing chemical reactions (sonochemistry). The NiO nanoparticles at different sizes have been characterized by X-ray powder diffraction (XRD), photo luminescent (PL) spectra and also the morphology and size of the nanostructures have been observed by scanning electron microscopy (SEM). We have performed these reactions in several conditions to find out the role of different factors such as the aging time of the reaction in the ultrasonic device and the concentration of the metal acetate on the morphology of nanostructures. However, from the most recent models concerning the QC effect in NiO nanocrystals and radiative states associated with the NiO interface, it is evident that the nanometer-sized NiO layer is essential to the PL characteristics of nanoscaled NiO nanoparticle systems. Even though examination of the optical properties of such extremely thin NiO sonochemical presents considerable challenge, experimental study of NiO-based nanomaterials by PL spectroscopy is intriguing, and spectral analysis to understand the origins of the observed PL features and their related dynamical mechanisms is far-reaching. In this article, we will discuss the PL from NiO-nanoparticles that we have investigated recently in our laboratory. In particular, we will show the blue-shifts of PL, originating from the electron–hole recombination of the self-trapped exciton (STE), in smaller-sized NiO-nanoparticles that we observed by PL spectroscopy. To explain the size effect in relating to the blue-shifts of STE PL, a question has been raised on whether it is appropriate to apply a QC model to wide band-gap material, such as silica. In this study, a laser-heating model of free excitons (FEs) to activate lattice phonons has been developed, rather than the QC effect, to illuminate the blue-shifts of STE PL in smaller-sized NiO-nanoparticles. The blue-shift resulted from the phonon-assisted STE PL in NiO-nanoparticles caused by the thermalization of the NiO-particle system due to frequent collisions between FEs and nanoscale boundary during laser irradiation.

2. Experimental

Typical procedure for preparation of NiO nanoparticles: NaOH solution with a concentration of 0.1 M (100 ml) was added to the 0.1 and 0.2 M solutions of $Ni(CH_3COO)_2{\cdot}2H_2O$ in ethanol/water. To investigate the role of surfactants on the size and morphology of nanoparticles, we used 0.5 ml of polyethylene glycol (PEG) in the reaction with optimized conditions. The mixtures were sonicated for 0.5, 1 and 2 h, with different ultrasound powers followed by centrifugation and separation of the solid and liquid phases. The solid phase was washed three times by ethanol and water. Finally, the washed solid phase was calcinated at 500 °C for 30 min. Table 1 shows the conditions of reactions in detail. A multiwave ultrasonic generator (Bandlin Sonopuls Gerate-Typ: UW 3200, Germany) equipped with a converter/transducer and titanium oscillator (horn), 12.5 mm in diameter, operating at 30 kHz with a maximum power output of 780 W, was used for the ultrasonic irradiation. The ultrasonic generator automatically adjusted the power level. The wave amplitude in each experiment was adjusted as needed. X-ray powder diffraction (XRD) measurements were performed using a Philips diffractometer of X'pert Company with mono chromatized Cukα radiation. The samples were characterized with a scanning

Table 1 Experimental conditions for the preparation of NiO nanoparticles.

Sample	$Ni(OAC)_2$	NaOH (0.1 M)	Aging time	Ultrasound power	Average size
1	25 ml (0.2 M)	100 ml	0.5 h	6–9 W	150 nm
2	25 ml (0.2 M)	100 ml	1 h	9–12 W	120 nm
3	25 ml (0.2 M)	100 ml	2 h	12–18 W	100 nm
4	50 ml (0.1 M)	100 ml	2 h	12–18 W	60 nm
5	50 ml (0.1 M)	100 ml	3 h	12–18 W	20 nm

electron microscope (SEM) (Philips XL 30) with a gold coating, to investigate the size distribution of the nanoparticles, a particle size histogram was prepared for NiO nanoparticles and most of the particles possess sizes in the range from 20 to 200 nm. The DTA and TGA data were obtained using a PL-STA 1500 apparatus and platinum crucibles with a heating rate of 5 °C min^{-1} in a static atmosphere of nitrogen. The EDAX spectrum given in shows the presence of Ni as the only elementary component in the NiO nanoparticles respectively. The use of PL is a routine analytical tool in many laboratories for impurity analysis, lattice properties and microstructure and we propose in this paper for size analysis of NiO nanoparticles.

3. Result and discussion

3.1. Theoretical discussion

The term ''nanotechnology'' has evolved over the years via terminology drift to mean ''anything smaller than microtechnology'' such as nano powder and other things that are nanoscale in size, but not referring to mechanisms that have been purposefully built from nanoscale components. This evolved version of the term is more properly labeled as ''nanoscale bulk technology,'' while retaining the original meaning of nanotechnology. Nanophase materials generally include original meaning is now properly labeled ''molecular nanotechnology'' (MNT), or ''nanoscale engineering,'' or ''molecular mechanics,'' or ''molecular machine systems,'' or ''molecular manufacturing.'' Recently, the Foresight Institute has suggested an alternate term to represent the nanocrystalline thin films, sintered materials with an ultra-fine gain structure and loosely aggregate nanoparticles. Size reduction affects most of the physical properties (structural, magnetic, optical, dielectric, thermal etc.) due to surface effects and quantum size effects. Owing to the extremely small dimensions these materials exhibit properties, which are fundamentally different from, and often superior to those of their conventional counterparts. The interest in the study of size effect in semiconductors of reduced dimensions (in nanometer scale) is due to their application in solar cells, light emitting diodes, resonant tunneling devices, laser catalyst etc. When the radius R of the crystallites is smaller than ~2 exciton Bhor radii, electrons and holes are considered as two confined particles bound by an enforced coulomb interaction and when crystallite radius is larger than ~4 exciton radii, the ground exciton is treated as a rigid sphere, confined as a quasiparticle. In between these two limiting cases both the electron and whole confinement and their coulomb interaction are considered. In case of nanocrystals, the electron, holes and exciton have limited space to move and their motion is possible for definite values of energy. As a result, the continuum of states in the conduction and valance band are broken down into discrete states with energy spacing relative to band edge, which is inversely proportional to the square of the particle radius resulting in the widening of the band gap as compared to the bulk. Quantum dots or nanoclusters exhibit discrete electron energy levels with high oscillator strength and strong luminescence. These systems have a very high surface to volume ratio and hence surface defects play an important role in their properties. The main aim of present paper is to analyze the size dispersion of nanoparticle that gives PL peak at different energies. As the optical properties are strongly dependent on particle size, a particle size distribution is expected to cause inhomogeneous broadening of optical spectra. The PL spectra often exhibit well defined peaks associated with band-edge luminescence and recombination at defects. These are also broadened in homogeneously due to particle size distribution; however there have been few attempts to analyze the spectra quantitatively. Here we will present a simple and elegant method for analysis of in homogeneously broadened band edge PL line shape for different particle size distributions. In order to keep the number of adjustable parameters minimum, the measured PL spectrum of bulk film is used as input. So considering the photoluminescence arising from the recombination of carriers at the band-edge in the bulk of direct-gap semiconductor with band-gap E_0. The resulting line shape can be represented by a Gaussian profile:

$$g_b(E) = A/\Gamma\sqrt{2\pi}exp[-(E-E_0)^2/2\pi^2] \tag{1}$$

where Γ is the parameter representing the intrinsic line width of the PL spectrum arising from the vibronic coupling. The full width at half maximum (FWHM) of Gaussian profile is equal to $(2.354)\ \Gamma$. Due to quantum confinement effect, the electronic energy levels of a semi-conductor nanoparticle (quantum dots) are shifted with respect to bulk. The lowest direct inter-band transition energy of a spherical quantum dot of radius R_0 has been obtained by Brus effective mass approximation as:

$$E(R_0) = E_0 + (h^2\pi^2/2)(1/m_e^* + 1/m_h^*)(1/R_0^2) - (1.8e^2/\varepsilon_2) - (1/R_0) + e^2/R_0\sum_{n=1}^{\infty}\alpha_o(S/R_0)^{2n} \tag{2}$$

where m_e^* and m_h^* are the effective mass of electron and holes respectively, e is the electron charge, ε_2 is dielectric constant of medium and α_n is a function of dielectric constant and S is electron–hole separation. The second term on the right hand side of Eq. (2) represents quantum localization energy. The third and the fourth terms correspond to coulomb potential and the polarization energy respectively. Hence blue shift in interband electronic transition is:

$$\Delta E(R_0) = E(R_0) - E_0 \quad (3)$$

In view of the shift of the direct interband transition energy, the PL spectrum of quantum-dot will also be shifted by same amount. The PL spectrum for nanoparticles of radius R_0 can thus be given by:

$$G_{gd}(E, R_0) = A/\Gamma\sqrt{2\pi g^*_{qd}(E, R_0)} \quad (4)$$

If the particle size is not uniform but has a distribution the observed spectrum of the quantum dot system can be taken as the superposition of the contribution from each individual particle. As each particle would exhibit a peak at a position dictated by its diameter, this would result in an inhomogeneous broadening of PL spectrum. The overall line shape can be determined by integrating g_{qd} (E,R) over size distribution $P(R)$ as:

$$G(E) = \int P(R).g_{qd}(E.R)dr \quad (5)$$

In order to keep calculation simple, the distribution $P(R)$ is taken to be Gaussian with mean R_0 and standard deviation σ_{R}.

$$P(R) = (1/\sigma_R\sqrt{2\pi})exp[-(R - R_0)^2/2\sigma_R^2)] = 1/\sigma_R\sqrt{2\pi P^*(R)} \quad (6)$$

Therefore:

$$G(E) = (A/2\pi\sigma_R\Gamma)\Sigma(R = R_0 - 3\sigma_R\, to\, R = R_0 + 3\sigma_R)[P^*(R)g_{db}(E.R)]dr$$

$$G(E) = F\Sigma(R = R0 - 3\sigma_R\, to\, R = R0 + 3\sigma_R)[P^*(R)g^*_{db}(E.R)]dr \quad (7)$$

3.1.1. PL peak broadening in NiO nanoparticles

Using Eq. (1) the line shape of bulk NiO can be obtained by substituting the constants for NiO. The constants that have been taken in present calculations are $\Gamma = 0.1$ and $E_0 = 2.70eV$. The value of A has been taken by, considering the maximum PL intensity, as unity i.e.:

$A/2\pi\Gamma\sigma_R = 1$ and $\Gamma = 0.1$

$A = 0.30$. Therefore this gives:

$$g_b(E) = (0.30/\sqrt{2 \times 3.14 \times 0.1})exp[-(E - 2.70)^2/2(0.1)^2]$$

For nanoparticles of average size 2 nm, $E(R)$ is first evaluated with the help of Eq. (2). Now $g_b(E)$ is calculated for different values of $E = 2.0, 2.1, \ldots, 3.8$. Now by using Eq. (4), the line shape of mono disperse NiO can be obtained by substituting value for $\sigma_R = 0.0001, m_e^* = 0.29, m_h^* = 0.75, \varepsilon_2 = 6.7, e = 1.9 \times 10^{-19}C, h = 7.70 \times 10^{-34}J - S$. To calculate the value for g_{qd} (E,R) it is necessary to find the value of $E(R_0)$ as shown below

$$E(R_0) = E_0 + (h^2\pi^2/2)(1/m_e^* + 1/m_h^*)(1/R_0^2) - (1.8e^2/\varepsilon_2) - (1/R_0) + e^2/R_0\sum_{n=1}^{\infty}\alpha_o(S/R_0)^{2n}$$

Here we see that for calculating $E(R_0)$, last term is neglected because its calculation is not straight forward.

$$E(R_0) = 2.43 + (h/2\pi)^2(\pi^2/2)(1/2.0 + 1/1.1)(1/2.2 \times 10^{-19} \times 9.1 \times 10^{-31} \times 10^{-18} \times R_0^2) - (1.8e^2/\varepsilon_2)(1/R_0)$$

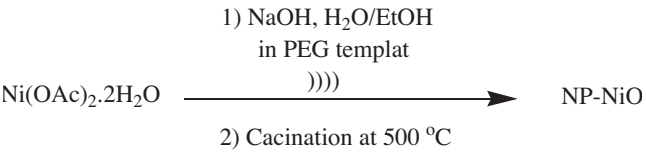

Scheme 1 The reaction between Ni acetate and sodium hydroxide to form NiO nanoparticles.

Now,

$$\varepsilon_2 = 4\pi\varepsilon_0\varepsilon_r = 6.7 \times 4\pi\varepsilon_0, \quad but \quad 4\pi\varepsilon_0(10^7/c^2)$$

Therefore:

$$(E, R_0) = 3.2 + (3.3/R_0^2) - (0.877/R_0)$$

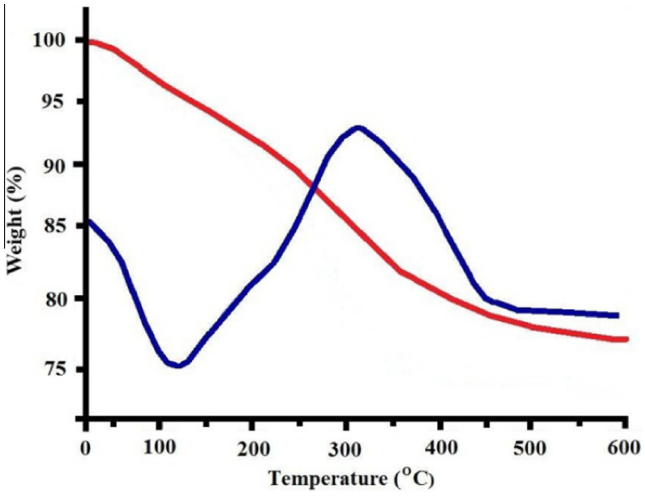

Figure 1 The TGA/DTA spectra of NiO nanoparticles (sample is random selected size of 100 nm).

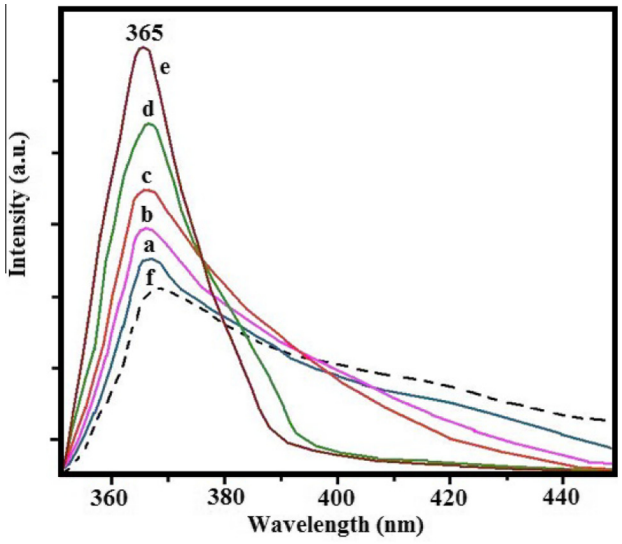

Figure 2 The solid state UV absorption of NiO nanoparticles at different size (a) 150 nm, (b) 120 nm, (c) 100 nm, (d) 60 nm, (e) 20 nm and (f) bulk size.

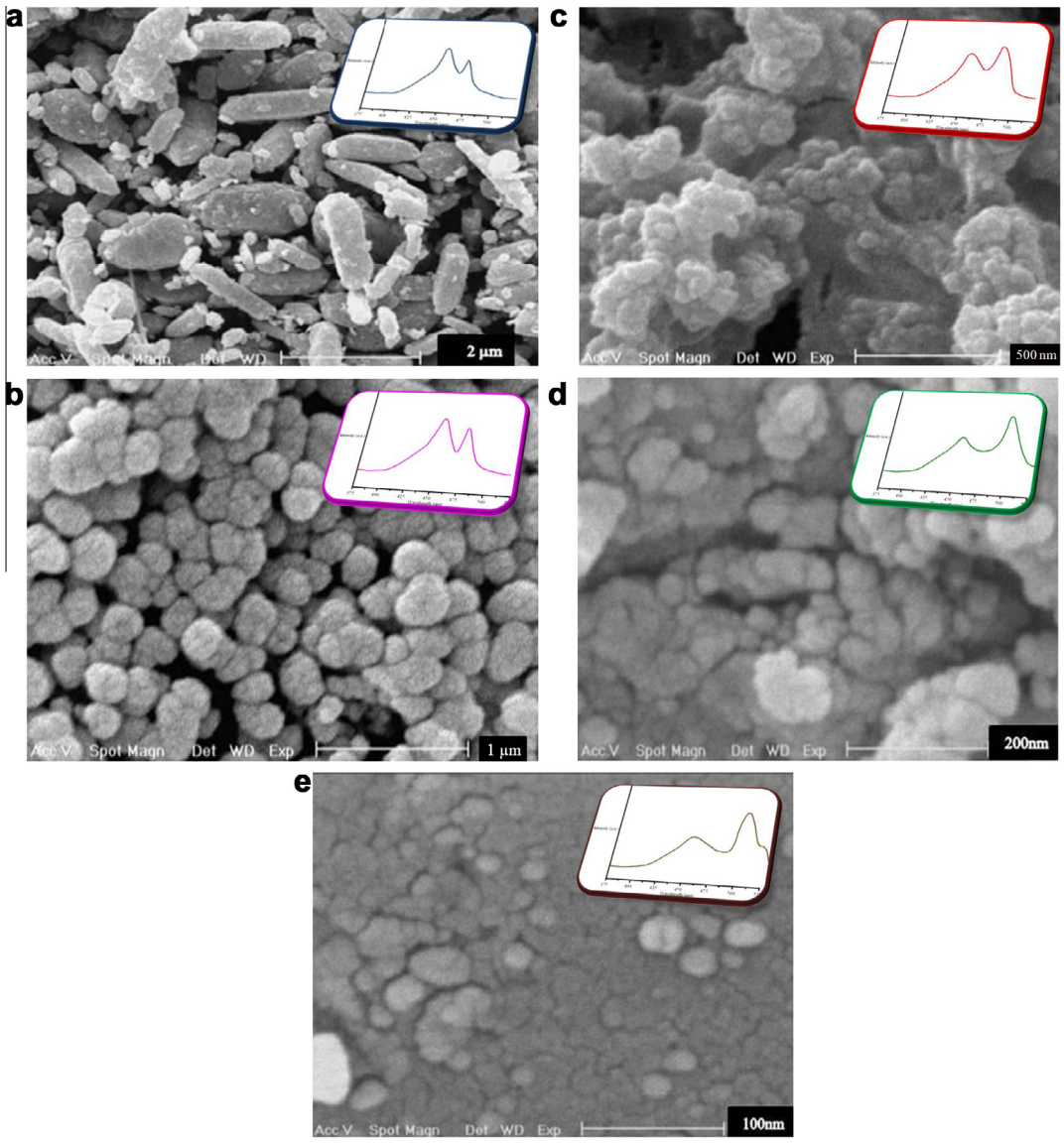

Figure 3 (a) Typical SEM micrographs of NiO nanoparticles at 150 nm size after calcinations. (b) Typical SEM micrographs of NiO nanoparticles at 120 nm size after calcinations. (c) Typical SEM micrographs of NiO nanoparticles at 100 nm size after calcinations. (d) Typical SEM micrographs of NiO nanoparticles at 60 nm size after calcinations. (e) Typical SEM micrographs of NiO nanoparticles at 20 nm size after calcinations.

From reported results it is found NiO with radius 1–4 nm the polarization term is typically one third of coulomb term with opposite sign. Therefore,

$$(0.3130/R) = (0.56/R) - (0.56/3R)$$

For NiO the value of $R_0 = 2\ nm$,

$$E(2) = 3.2 + (3.3/2^2) - (0.3130/2) = 4.61eV$$

Substituting the value of Γ, A and $E(R_0)$, for different values of E, $g_{qd}(E,R_0)$ is calculated by Eq. (4) NiO.

Using Eqs. (2) (4) (6) and (7), the line shape of polydisperse NiO can be obtained by substituting the constants for NiO nanoparticles. Following constants are in present calculation.

$$(\sigma_R/R_0) = 25\%, (a/2\pi\Gamma\sigma_R) = F = 0.9,\ dR = 0.2,$$
$$R = 0.5\ to\ 4nm$$

Substituting the above values in Eq. (7), $P^*(R)$ is calculated for different values of $R = 0.5$ to 4 nm. Similarly $E(R)$ is calculated by Eqs. (8) and (9) energy $R = R_0 + 3\sigma_R$ for different values of $R = 0.5\ to\ 4\ nm$. Then $g^*_{qd}(E.R)$ is calculated by Eq. (4) for different values of E. Substituting the value $P^*(R)$ and $g^*_{qd}(E.R)$ for specific value of R and E in Eq. (6). Substituting $dR = 0.2$, $[(a/2\pi\Gamma\sigma_R) = 0.8]$ we get different values of $g^*_{qd}(E,R)XP^*(R)XFXdR$. The Eq. (5) for NiO is given by [polydisperse] (Zhang et al., 2006; Sun, 2002; Kumar and Kim, 2006; Srinivasan and Weidner, 1997; Kingery et al., 1976).

$$(\sigma_R/R_0) = 15\%, (A/2\pi\Gamma\sigma_R) = F = 1.3, dR = 0.1,$$
$$R = 1.1\ to\ 2.9nm$$

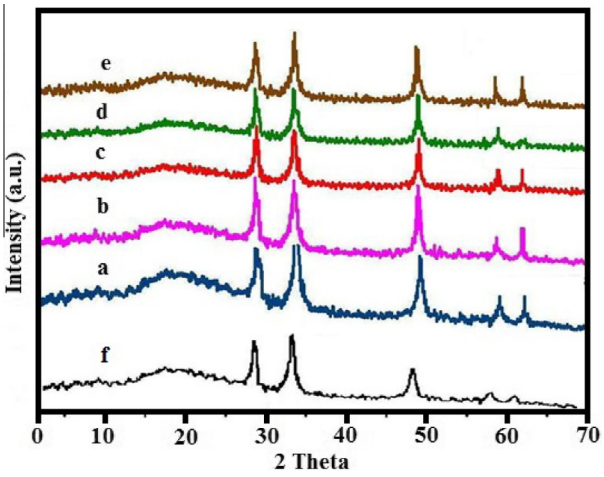

Figure 4 The X-ray powder diffraction pattern of NiO nanoparticles (a) NiO at 150 nm, (b) NiO at 120 nm, (c) NiO at 100 nm, (d) NiO at 60 nm, (e) NiO at 20 nm and (f) NiO at bulk size.

3.2. Experimental discussion

The reaction between Nickel acetate and sodium hydroxide to form NiO nanoparticles has been shown in Scheme 1.

Various conditions for preparation of NiO nanostructures were summarized in Table 1.

In order to reveal the changes that occurred during heat treatment of the precursor powders, TG and DTA analyses were carried out from 25 to 600 °C in atmosphere (see Fig. 1). According to the TG curve, the major part of the weight loss seems to occur below 350 °C. DTA curve shows an endothermic peak at about 121 °C, corresponding to the evaporation of the absorbed water. An exothermic peak at approximately 314 °C occurs in DTA, which might be associated with the conversion of precursor into NiO and also the decomposition of the organic residues. The reaction is completed by 450 °C. Therefore, we choose 450 °C as the calcine temperature.

When the semiconductor particles are sufficiently small and the radius of the particle approaches the radius of the first excited-state orbital of the conduction band electrons, the so-called quantum-size effects are observed. With reduction in particle size, the band gap of the semiconductor becomes larger and there is a concomitant blue shift in the absorption spectrum. The UV–Vis spectra of NiO nanoparticles are shown in Fig. 2. It is noticed the phenomenon of the blue shift, with the decrease of R value, which is an evidence of quantum confinement effect, which implies that with the increase of R value the particles size became larger.

The solid state UV–Vis spectrum of nanoparticles and NiO at bulk size displays an absorption band with maximum intensity at 360 nm Fig. 2(a–f), whereas NiO nanoparticles display one absorption sharp band with maximum intensity at 365 nm. But the bulk NiO powders have very limited UV absorbance, and absorbance in the UV region is enhanced with

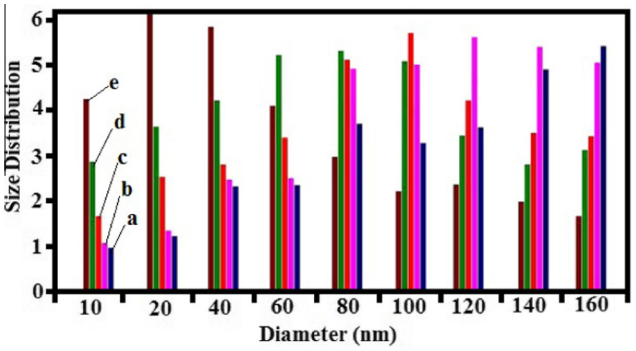

Figure 5 Particle size histogram of NiO with different size (a) 150 nm, (b) 120 nm, (c) 100 nm, (d) 60 nm and (e) 20 nm.

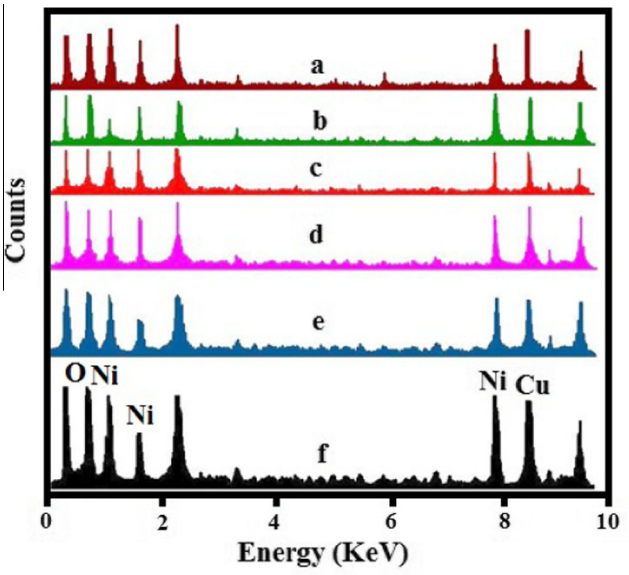

Figure 6 The EDAX analysis of NiO nanoparticles and bulk size (a) 150 nm, (b) 120 nm, (c) 100 nm, (d) 60 nm, (e) 20 nm and (f) bulk size.

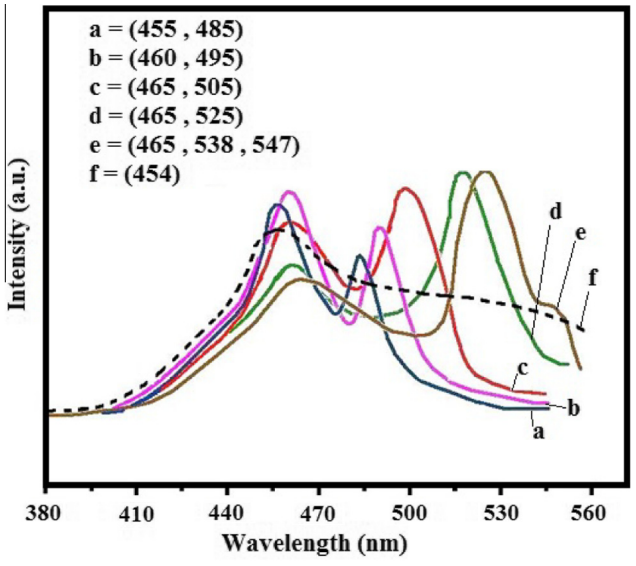

Figure 7 The solid state PL analysis of NiO nanoparticles at different size (a) 150 nm, (b) 120 nm, (c) 100 nm, (d) 60 nm, (e) 20 nm and (f) bulk size. (λ_{ex} = 360 nm).

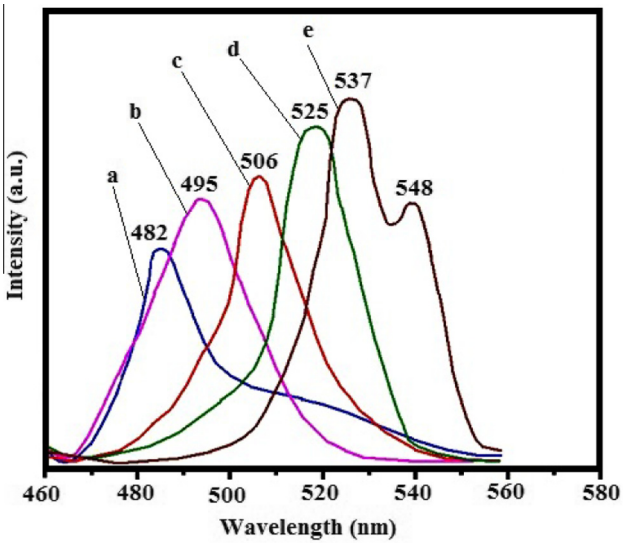

Figure 8 The solid state PL analysis of NiO nanoparticles at different size (a) 150 nm, (b) 120 nm, (c) 100 nm, (d) 60 nm, (e) 20 nm. (λ_{ex} = 460 nm).

the NiO nanoparticles at different sizes due to its high energy gap. Nanoparticles under 200 nm have better transmission of visible light compared to NiO at bulk size. The optical absorption peak intensity is found at 3.39 eV (365 nm). From the curve we can calculate the band gap (E_g) energy of the sample by the following equation:

$$(\alpha h\nu)^n = B(h\nu - E_g)$$

where hν is photo energy, α is absorption coefficient, B is a material constant and n is either 2 for a direct band gap material or ½ for an indirect band gap materials that we know NiO is a direct band gap type semiconductor. A typical SEM image in Fig. 3 showed the morphology and size of the NiO nanoparticles prepared by sonochemical method with different R values. It follows that the average size of the nanoparticles increased with increasing R value. The morphology, structure and size of the samples are investigated by scanning electron microscopy (SEM). Fig. 3(a–e) indicates that the original morphology of the NiO nanoparticles is approximately spherical with the diameter varying between 10 and 200 nm. This is consistent with the UV–Vis spectra results. The best morphology with smaller particles and good distribution was obtained for the samples summarized. Fig. 4(a–f) shows the XRD patterns of the direct sonochemically synthesized NiO nanoparticles respectively. Sharp diffraction peaks shown in Fig. 4 indicate good crystalline of NiO nanoparticles. No characteristic peak related to any impurity was observed. The broadening of the peaks indicated that the particles were of nanometer scale.

To investigate the size distribution of the nanoparticles, a particle size histogram was prepared for NiO nanoparticles, Fig. 5(–e). For further demonstration the EDAX was performed for the NiO nanoparticles. The EDAX spectrum given in Fig. 6(a–e) shows the presence of Ni as the only elementary component in the NiO nanoparticles respectively. Bulk and nanoparticle powder of NiO at different sizes was analyzed by solid state photo-luminescent (PL) spectrum for preparation of their emissions. The PL can be produced from sources such as quantum confinement and surface states. On the other hand photoluminescence spectroscopy is usually used to measure the band-gap energy of semiconductors. Therefore, we focus on the photoluminescence spectrum of NiO semiconductor nanoparticles in this study. NiO at bulk size exhibits one fluorescence emission maxima at 454 nm upon photo excitation at 360 nm (Fig. 7(a–f)). Compared to the fluorescence signals of nanoparticles of NiO at different sizes two fluorescence emission maxima at 455 (2.72 eV) and 485 nm (2.55 eV) for 150 nm, 460 nm (2.69 eV) and 495 nm (2.50 eV) for 120 nm, 465 nm (2.66 eV) and 505 nm (2.45 eV) for 100 nm, 465 nm (2.66 eV) and 525 nm (2.36 eV) for 60 nm and 465 (2.66 eV), 538 (2.30 eV) and 547 nm (2.26 eV) for 20 nm. The fluorescence spectra of nanoparticles with λ_{exc} = 360 nm are shown in Fig. 7(a–f). Hexagonal phase NiO nanoparticles at different sizes exhibit the same emission position at 454 nm for bulk size of NiO and 485 nm for NP-NiO at 150 nm in 485 nm, for NP-NiO at 120 nm in 495 nm, for NP-NiO at 100 nm in 505 nm, for NP-NiO at 60 nm in 525 nm and for NP-NiO at 20 nm in 538 and 547 nm. Therefore, we can observe that decrease in the size of nanoparticles from 150 to 20 nm causes decrease in the photoluminescence (PL) spectral energy. However, the emission intensity of NP-NiO nanoparticles with different sizes is greater than that of bulk size of NiO powders. Is the difference of the emission intensity due to the size or morphology? To investigate the reason, the contradistinctive experiment was carried out under sonochemical condition. It indicates that the emission intensity of NP-NiO with different sizes is greater than that of bulk size of NiO. This suggests that the size is the main factor leading to the difference of emission intensity. It is thought that the difference of the emission intensity likely depends on their variation size and morphology. The fluorescence spectra clearly suggest that nanoparticles of NiO are a son ably luminescent material and probably this property can be exploited for possible future applications. The fluorescence spectra of nanoparticles with λ_{exc} = 460 nm are shown in Fig 8(a–f). In this case the PL spectra have a single peak, with nearly broad full width at half maximum (FWHM). These peaks located in 2.57 eV for 150 nm particle size, 2.50 eV for 120 nm, 2.45 eV for 100 nm, 2.36 eV for 60 nm, 2.30 eV for 20 nm of NiO particle size. The intensity of PL spectrum gradually increases from 150 to 20 nm particle size and the energy band gap decreases from 150 nm to 20 nm of NP-NiO for λ_{exc} = 460 nm. In other words, the blue shift occurs due to reduced size of NP-NiO.

4. Conclusion

Many workers have reported band to band PL for a number of materials. In case of nanocrystals the PL peak is observed at same energy as the absorption edge shifts toward shorter wavelength for smaller particles. In general it is difficult to obtain monodisperse particles and PL spectrum can be taken as superposition of the contribution from each individual nanoparticle. The effect of particle size distribution of semiconductor nanoparticles on the band-edge photoluminescence spectrum is investigated. The calculations show inhomogeneous broadening of PL line shape. The measured PL spectrum which exhibits peaks arising from band-edge luminescence and recombination at defects can be analyzed by fitting the calculated line shape to it. Thus, the overall

behavior of PL spectrum is strongly affected by the size distribution of nanoparticles.

In summary we suggest that the PL spectrum is the simple, straight and inexpensive method for preparation of size in nanoparticles of NiO. Nanoparticles of NiO are various emissions responsive they size and morphologies. However the different sizes of nanomaterials have various emissions in PL spectra and this demonstrates that photoluminescence spectroscopy can be a powerful method for grading of NiO nanoparticles.

Acknowledgments

Supporting of this investigation by the Jundi-Shapur University of Technology, Dezful, Iran and Nanobiotechnology research center of Baqiyatallah University of Medical Science, Tehran, Iran and Ataturk University of Erzurum, Turkiye, is gratefully acknowledged. Finaly, This work Proffer to, Prof. Dr. Masoud Alimohammadi, Prof. Dr. Majid Shahriyari, Mr. Mostafa Ahmadi-Roshan and Mr. Dariush Rezayinejad, Dr. Hassan Tehrani-Moghaddam and Prof. Dr. VESEL TURAN YILMAZ.

References

Bandara, J., Yasomanee, J.P., 2007. Semiconductor Sci. Technol. 22, 20–24.

Buffat, P.H., Burrel, J.P., 1976. Phys. Rev., 2287.

Curri, M.L., Agostiano, A., Mavelli, F., et al., 2002. Mater. Sci. Eng., C, Biomim. Mater., Sens. Syst. 22, 423.

He, J., Lindström, H., Hagfeldt, A., Lindquist, S.-E., 1999. J. Phys. Chem. 103, 8940.

Jiang, L., Sun, G., Zhou, Z., Sun, S., Wang, Q., Yan, S., Li, H., Tian, J., Guo, J., Zhou, B., Xin, Q., 2005. J. Phys. Chem. B 109, 8774.

Karar, N., Singh, F., 2004. J. Appl. Phys., 650.

Kingery, W.D., Bowden, H.K., Uhlmann, D.R., 1976. Wiley Series on the Science and Technology of the Materials, second ed. Wiley, New York, p. 1032.

Kumar, V.G., Kim, K.B., 2006. Ultrason. Sonochem. 13, 549.

Lei, H., Tang, Y.-J., Wei, J.-J., Li, J., Li, X.-B., Shi, H.-L., 2007. Ultrason. Sonochem. 14, 81.

Liao, C.L., Lee, Y.H., Chang, S.T., Fung, K.Z., 2006. J. Power Sources 158, 1379–1385.

Liu, K., Anderson, M., 1996. J. Electrochem. Soc. 143, 124.

Maeda, Y., Tssukamoto, N., 1991. Appl. Phys. Lett. 59, 3138.

Mao, Chang-Jie, Pan, Hong-Cheng, Wu, Xing-Cai, Zhu, Jun-Jie, Chen, Hong-Yuan, 2006. J. Phys. Chem. B 110, 14709.

Pejova, B., Kocareva, T., Najdoski, M., Grzdanov, I., 2000. Appl. Surf. Sci. 165, 271.

Sato, H., Minami, T., Takata, S., Yamada, T., 1993. Thin Solid Films 236, 27.

Song, Q.S., Li, Y.Y., Chan, S.L.I., 2005. J. Appl. Electrochem. 35, 157.

Srinivasan, V., Weidner, J., 1997. J. Electrochem. Soc. 144, L210.

Sun, Y., Xia, Y., 2002. Science 298, 2176–2179.

Suslick, K. S. "Sonochemistry," in Kirk-Othmer Encyclopedia of Chemical Technology; 4th Ed., J. Wiley & Sons: New York, 1998, vol. 26, 517–541. Suslick, K. S.

Suslick, K.S., Fang, M., Hyeon, T., 1996. J. Am. Chem. Soc. 118, 11960.

Wang, S.F., Gu, F., Lü, M.K., 2006. Langmuir 22, 398.

Wang, H., Wong, K.S., Wong, G.K.L., 1998. J. Appl. Phys. 83, 4773.

Xu, J.-Z., Xu, S., Geng, J., Li, G.-X., Zhu, J.-J., 2006. Ultrason. Sonochem 13, 451.

Yu, J.C., Yu, J., Zhang, L., Ho, W., 2002. J. Photochem. Photobiol. A: Chem. 148, 263.

Zhang, S.-Y., Liu, Y., Ma, X., Chen, H.-Y., 2006. J. Phys. Chem. B 110, 9041.

Zhou, H., Zhou, Z., 2005. Solid State Ionics 176, 1909.

Zhu, J., Lu, Z., Aruna, S.T., Aurbach, D., Gedanken, A., 2000. Chem. Mater. 12, 2557.